nanomaterials

MDPI

Article

Nanotextured CeO_2-SnO_2 Composite: Efficient Photocatalytic, Antibacterial, and Energy Storage Fibers

Jari S. Algethami [1,2], M. Shamshi Hassan [3,*], Touseef Amna [4,*], Faheem A. Sheikh [5], Mohsen A. M. Alhamami [1], Amal F. Seliem [1], M. Faisal [1,2] and H. Y. Kim [6]

1 Department of Chemistry, College of Science and Arts, Najran University, Najran 11001, Saudi Arabia
2 Promising Centre for Sensors and Electronic Devices (PCSED), Advanced Materials and Nano-Research Centre, Najran University, Najran 11001, Saudi Arabia
3 Department of Chemistry, College of Science, Albaha University, Albaha 65799, Saudi Arabia
4 Department of Biology, College of Science, Albaha University, Albaha 65799, Saudi Arabia
5 Nanostructured and Biomimetic Lab, Department of Nanotechnology, University of Kashmir Hazratbal, Srinagar 190006, India
6 Organic Materials and Fibers Engineering Department, Chonbuk National University, Jeonju 560011, Republic of Korea
* Correspondence: hassan4nano@gmail.com (M.S.H.); touseefamna@gmail.com (T.A.); Tel.: +966-536913920 (M.S.H.)

Abstract: Bacterial infections remain a serious and pervasive threat to human health. Bacterial antibiotic resistance, in particular, lowers treatment efficacy and increases mortality. The development of nanomaterials has made it possible to address issues in the biomedical, energy storage, and environmental fields. This paper reports the successful synthesis of CeO_2-SnO_2 composite nanofibers via an electrospinning method using polyacrylonitrile polymer. Scanning and transmission electron microscopy assessments showed that the average diameter of CeO_2-SnO_2 nanofibers was 170 nm. The result of photocatalytic degradation for methylene blue dye displayed enhanced efficiency of the CeO_2-SnO_2 composite. The addition of SnO_2 to CeO_2 resulted in the enhancement of the light absorption property and enriched charge transmission of photoinduced electron–hole duos, which conspicuously contributed to momentous photoactivity augmentation. Composite nanofibers exhibited higher specific capacitance which may be accredited to the synergism between CeO_2 and SnO_2 particles in nanofibers. Furthermore, antibacterial activity was screened against *Escherichia coli* and CeO_2-SnO_2 composite nanofibers depicted excellent activity. The findings of this work point to new possibilities as an electrode material in energy storage systems and as a visible-light-active photocatalyst for the purification of chemical and biological contaminants, which would substantially benefit environmental remediation processes.

Keywords: CeO_2-SnO_2; environmental remediation; antimicrobial; photocatalyst; supercapacitor

Citation: Algethami, J.S.; Hassan, M.S.; Amna, T.; Sheikh, F.A.; Alhamami, M.A.M.; Seliem, A.F.; Faisal, M.; Kim, H.Y. Nanotextured CeO_2-SnO_2 Composite: Efficient Photocatalytic, Antibacterial, and Energy Storage Fibers. *Nanomaterials* **2023**, *13*, 1001. https://doi.org/10.3390/nano13061001

Academic Editor: Andreu Cabot

Received: 9 February 2023
Revised: 1 March 2023
Accepted: 7 March 2023
Published: 10 March 2023

1. Introduction

Globally, environmental pollution is a serious problem, inflicting harm to life on the planet. Water pollution, among other types of pollution, has a significant negative impact on living species, including aquatic life. Water pollution is due to the discharge of harmful organic chemicals, such as dyes, acids, and antibiotics, into drinkable water bodies, such as rivers, lakes, and ponds, from textile, chemical, and pharmaceutical facilities. In nature, the majority of organic molecules are carcinogenic. Furthermore, water pollution sequentially causes soil pollution, which has a direct or indirect impact on daily living [1,2]. Synthetic color dyes, particularly those generated during textile washes, combine easily with water in comparison to chemicals and reagents; hence, the combination of effluents has hazardous potential. As a result, industrial effluent must be processed prior to being disposed of in the surroundings [3]. Dyes are colored aromatic organic complexes that capture light

and provide color [4]. Because of these advantages, various dyes are utilized for a variety of applications in commerce, such as fabrics, foodstuffs, rubber, lithography, makeup, medication, plastic, concrete, and paper. Companies produce massive amounts of effluent, including carcinogenic and poisonous dyes, that pollute water and render it unsafe for human consumption. The textile sector is the largest dye-consuming business, relying on textile dyes, which are very complex molecules [5].

Methylene blue (MB), which is extensively used to color different fabrics, such as silk, wood, and cotton, as well as paper, is one of the most consumed ingredients in dye commerce [6]. Textile manufacturers typically release a considerable amount of MB dyes into natural water reservoirs, imposing health threats to beings and microbes [7]. Owing to its extreme toxicity, MB dye is dangerous to human health above a specific content level. MB is toxic, cancer-causing, and non-biodegradable, and it can put human well-being in danger and has a deleterious influence on the environment [7]. Human health dangers from MB comprise respiratory agony, gastrointestinal problems, vision, and digestive and mental illnesses [8]. Additionally, it produces indigestion, diarrhea, vomiting, cyanosis, dizziness, gastritis, jaundice, methemoglobinemia, tissue necrosis, and an escalation of heart rate, as well as untimely cell death in tissues and skin/eye irritability [7,9]. Contact with MB might cause skin redness and irritation [10]. For both aesthetic and toxicological reasons, MB liberation into surroundings poses a considerable concern. The management of wastewater containing MB dye before discharge into the environment is critical because of the negative effects on water quality and perception [11].

Likewise, major bacterial diseases are transmitted through wastewater. Therefore, microbiological management of drinking water should be the standard everywhere. Additionally, regular basic microbiological analysis of drinking water should be performed using culture methods to perceive the presence of pathogenic *Escherichia coli.* Hygienic water is essential for life, but an enormous number of persons are deprived of access to potable water, and many die as a result of waterborne bacterial infections [12]. To date, many water treatment technologies, including biodegradation, coagulation, adsorption, and photocatalysis, have been used to remove organic pollutants [13]. Multi-constituent photocatalysis of organic contaminants utilizing semiconducting NPs has gained popularity in recent decades because it is a low-cost, ecologically beneficial, and simple technology for treating dangerous contaminants in wastewater [4,14,15]. When compared with other ways, this technology is much more appealing due to the cheaper price of catalysts and the use of renewable energy [16].

One-dimensional (1D) nanostructured inorganic materials, especially nanofibers, are attracting a lot of attention. They were applied in various applications recently. One-dimensional metal oxides, as well as hybrids or composites [17], provide a wide range of material options, providing new options for future applications [18,19]. Electrospinning is one of the best flexible, multipurpose, and economical techniques that produce 1D nanofibers with a high aspect ratio, permeability, and adjustable penetrability. Remarkable progress was also made toward the utilization of such purposeful nanofibers in practical applications, such as fuel cells, lithium-ion arrays, solar booths, electronic sensors, photocatalysts, and supercapacitors [20]. Given the importance of renewable energy that is environmentally friendly, supercapacitors are in high demand; mostly because of their robust charge–discharge capacity, these supercapacitors are reliable [20].

Electrospinning has notable capability because of its proportionally low cost and relatively fast fabrication speed [21–24]. In recent years, cerium oxide (CeO_2) has received significant attraction owing to its diverse properties, such as high-temperature stability and light absorption capability, as well as its broad range of catalytic applications [25–27]. It absorbs light in both the UV and visible regions; it was also applied as an effective oxidation catalyst, as it has high oxygen storage capability [28]. Moreover, it is also being used for the degradation of dyes and volatile organic compounds (VOCs) [29,30]. Currently, CeO_2 is used as a photocatalyst and as an electrode material for supercapacitors [31,32]. Researchers are trying to enhance the properties of CeO_2 for various applications by mixing

or coupling with other semiconductors, such as $CeO_2/ZnFe_2O_4$ [33], TiO_2-WO_3-CeO_2 [34], CeO_2/Ni-Al [35], CeO_2/MnO_2 [36], CeO_2/SiO_2 [37], CuO-CeO_2 [38], CaO/CeO_2 [39].

Tin oxide (SnO_2) is an n-type semiconductor with a band gap of 3.6 eV. SnO_2 has extensively been utilized as gas sensors, transparent conductive electrodes, solar cells, and photocatalysts [40–42]. It is expected that mixing SnO_2 with CeO_2 may enhance its activity for various applications. In the present study, CeO_2-SnO_2 composite nanofibers (NFs) were manufactured via electrospinning and screened for antibacterial, photocatalytic, and electrochemical applications. For decades, antibiotics have commonly been used to treat bacterial infections. However, the fast growth of antibiotic-resistant bacteria has caused several issues that place a significant burden on the medical community. As a result, the use of nanoparticles as an antibacterial substitute has been investigated. Regarding this situation, metal nanoparticles showed broad-spectrum antibacterial action. Furthermore, the use of nanomaterials in the biomedical area allows researchers to solve the issues of bacterial antibiotic resistance due to their distinct antibacterial mechanisms. Several metal and metal oxide-based nanomaterials were recently fully integrated into antibacterial applications and demonstrated remarkable performances [43]. Among them, Ce- and CeO_2-based nanomaterials garnered a lot of attention across the world. Numerous investigations demonstrated that CeO_2 nanoparticles have remarkable antibacterial activity [44,45]. Several investigations showed that CeO_2 has an antibacterial impact on *Staphylococcus aureus* [46,47]. Furthermore, some research studies used agar diffusion and microdilution assays to investigate and confirm *P. aeruginosa*'s sensitivity to CeO_2 [48]. In the same way, SnO_2 also received attention as an antibacterial agent, where it was shown to inhibit the development of several bacterial strains, such as *S. aureus* and *E. coli* [49,50]. Furthermore, it was also found that SnO_2 disinfects germs effectively once incapacitated with transition metal ions, for instance, Co@SnO_2 and Ag@SnO_2 nanoparticles exhibit powerful antimicrobial properties [51–53].

However, to the best of our knowledge, no research work has been published on the antibacterial behavior of CeO_2-SnO_2 composite NFs. This paper describes the facile manufacturing of CeO_2-SnO_2 composite NFs via electrospinning and their incredible photocatalytic, electrochemical applications, and antibacterial activity against *E. coli.* The composite was categorized using various physicochemical techniques, such as XRD, SEM, TEM, FT-IR, PL, and UV-vis. The photocatalytic activity was measured using MB disintegration under visible light radiation. The mechanism of improved photocatalytic activity of composite CeO_2-SnO_2 NFs was interpreted. The electrochemical efficiency of synthesized materials was scrutinized in terms of the cyclic voltammetry performance, which displayed that the CeO_2-SnO_2 composite possessed outstanding electrochemical efficacy as a supercapacitor material. Overall, the outcomes of this research highlight the innovative possibilities of utilizing these 1D high-aspect-ratio composite NFs as an electrode in energy storage systems and as a visible light active photocatalyst for the purification of chemical and biological contaminants, which would greatly assist in environmental remediation procedures. Henceforward, composites of these two materials (CeO_2-SnO_2) can serve as an excellent preliminary point for augmenting electrodes and photocatalytic efficiency. Additionally, this combination will be an imminent antimicrobial material with multiple functionalities. To recapitulate, the novelty of this work is that we used a facile electrospinning technique to fabricate composite NFs using cost-effective precursors. The CeO_2-SnO_2 composite NFs with a high aspect ratio are an auspicious future material and can be applied for antibacterial, photocatalyst, and electrode purposes, all in one.

2. Materials and Methods

2.1. Synthesis of Pure CeO_2 and CeO_2-SnO_2 Composite NFs

Pristine CeO_2 NFs were fabricated via an electrospinning process devoid of tin(II)ethylhexanoate in sol-gel. A polyvinylpyrrolidone (PVP, 15 wt%) solution was made via the usual technique by melting PVP in dimethylformamide (DMF) under magnetic stimulation for 5 h at room temperature. $Ce(NO_3)_3 \cdot 6H_2O$ (1.0 g) was then added to the PVP solution while

vigorously shaking. The resulting sol-gel was electrospun. The samples were subsequently sintered in air for 2 h at 500 °C to eliminate the polymer.

In the general process, for the synthesis of CeO_2 and CeO_2-SnO_2 composite NFs, PVP (15 wt%) solution was primed by liquefying PVP in DMF on a magnetic stirrer as abovementioned. Tin(II) ethylhexanoate (0.15 mL) was supplemented with 2 mL of ethanol, then transferred into 10 mL of PVP solution. $Ce(NO_3)_3 \cdot 6H_2O$ (1.0 g) was added to produce the final solution. The acquired sol-gel was transported into a 10 mL needle with a stainless steel spike. A copper pin coupled to a high voltage generator was implanted in solution as a positive terminal, while a ground iron barrel roofed with a polyethylene leaf assisted as the counter electrode. The mixture was retained as a capillary by regulating the inclination angle. A voltage of 17.5 kV was maintained to produce the final resultant assortment. The distance between the tip of the needle and the collector was held at 15 cm. Primarily, as-spun composite NFs were desiccated at 80 °C for 24 h in a vacuum. Additionally, to eliminate the polymer, composites were calcined in air at 500 °C at a rate of 2 °C/min for 2 h.

2.2. Classification of Pure CeO_2 and CeO_2-SnO_2 NFs

The XRD outlines of pure and composite NFs were measured using a Rigaku/Max-3A (Tokyo, Japan) with Cu Kα radiation (λ = 1.540 Å) over Bragg angles between 20° to 80°. To scan surface features, pristine and composite NFs were examined using field emission scanning electron microscopy (FE-SEM, JSM6700, JEOL, Tokyo, Japan) and high-resolution transmission electron microscopy (HRTEM-H-7650 Hitachi, Co., Tokyo, Japan). The elemental conformation of the samples was scrutinized using energy-dispersive X-ray spectroscopy (EDS) coupled to an SEM instrument. The EDS of the sample was taken on carbon tape with a Pt coating. The photoluminescence (PL) spectra of the NFs were measured at room temperature using the 325 nm line of a He-Cd laser at a power of 25 mW for excitation (Kimmon Koha, JP/IK 3302 R). The light absorbance of NFs was measured by means of a UV-vis diffused reflectance spectrum (UV-DRS, 525 Shimadzu).

2.3. Photocatalytic Degradation

Photocatalytic activity of CeO_2-SnO_2 composite has been performed by disintegration of MB dye in visible light treatment using 450 W Xenon lamp. In 250 mL of a solution, there was a dye concentration of 10 mgL^{-1} and 250 mg of photocatalyst; this was stirred for 1 h in the dark (at a neutral pH). Afterward, around 3 mL of aliquots was taken at regular time intervals from the solution and centrifuged. The absorbance of MB dye mixture was analyzed by a UV–Vis spectrophotometer (Shimadzu UV-3101, UV Probe) at a 664 nm absorbance peak.

2.4. Electrochemical Characterization

Cyclic voltammetry was undertaken in a three-electrode configuration by means of a potentiostat (Digi-Ivy, USA). A glassy carbon electrode was used, while Ag/AgCl and Pt were used as the working standard and the counter electrode, respectively. The specific capacitance (Cs) was measured from CV curves calculated graphically by integrating the area under the CV curve with help of the following equation [54]:

$$Cs = \int_{Va}^{Vc} IVdV \frac{1}{w \times \upsilon \times (Va - Vc)} \quad (1)$$

where w is the mass of the electrode and υ is the sweep rate (V/s).

2.5. Antimicrobial Activity

The antimicrobial actions of CeO_2 and CeO_2-SnO_2 composite NFs were screened against *E. coli*, which is ever-present throughout the atmosphere. The bacterial standard cultures were held on nutrient agar (NA) plates. Bacterial culture from the agar plates was

seeded in 5 mL NS solution and adjusted to 1×10^6 CFU/mL. To evaluate the antibacterial effect, different concentrations of CeO_2 NFs and CeO_2-SnO_2 composite NFs were prepared and screened. Preliminary screening was conducted using an agar diffusion technique, as described previously [55]. In short, 25 mL of agar holding 1 mL of microbial culture was placed in Petri dishes. Approximately 50 µL from each dosage was put into a 4 mm diameter well. Dishes were pre-incubated for 3 h at room temperature to enable the pre-diffusion of samples and then incubated for 24 h at 37 °C. As a negative control, DMSO was utilized, and the standard drug ciprofloxacin was used as the positive control. The inhibition potency was described as the absence of bacterial growth in the vicinity of holes and a caliper was used to determine the inhibition zone.

3. Results and Discussion

Electrospinning is a simple and versatile technology that uses electrostatic repulsion between surface charges to extract nanofibers from a viscoelastic fluid and can be used for a variety of materials [56]. In the present study, it was utilized successfully to make composite NFs with diameters as small as hundreds of nanometers. The XRD configuration of CeO_2 and CeO_2-SnO_2 NFs after calcination at 500 °C are displayed in Figure 1. Specifically, all of the reflection crests in Figure 1a were assigned to the cubic fluorite structure of CeO_2 (JCPDS no. 65-2975) at angles of 28.5°, 33.2°, 47.5°, 56.4°, and 59.1°, which relate to the (111), (200), (220), (311), and (222) crystal planes, respectively [26]. A small peak was observed at 52.5°, which was probably the peak of $Ce(OH)_3$ [57]. In the XRD configuration of CeO_2-SnO_2 (Figure 1b), major diffracted crests identical to those of CeO_2 NFs were visualized. Additionally, diffraction peaks from the tetragonal SnO_2 (JCPDS card no. 41-1445) were also observed [58], which demonstrates the effective materialization of CeO_2-SnO_2 composite NFs. No other mixes of Ce and Sn were detected using XRD.

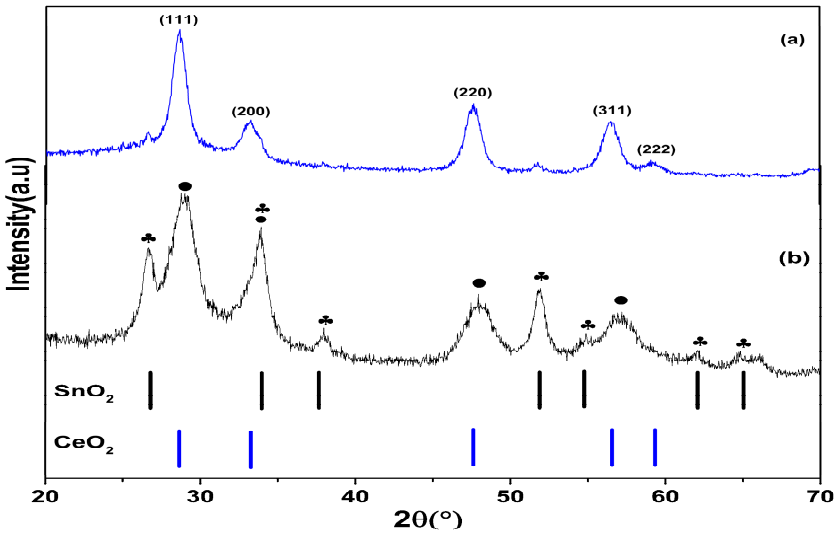

Figure 1. XRD patterns of (**a**) CeO_2 and (**b**) CeO_2-SnO_2 composite NFs calcined at 500 °C.

The morphologies of pure and composite NFs obtained after heating at 500 °C were demonstrated using SEM (Figure 2). From Figure 2a, it can be perceived that these arbitrarily oriented NFs had a uniform and continuous structure. Their lengths were measured as being several micrometers. The average diameter of the pure CeO_2 NFs was 400 nm, whereas the average diameter of CeO_2-SnO_2 composite NFs was lower at 170 nm, which might have been due to the interaction between Ce and Sn (Figure 2b).

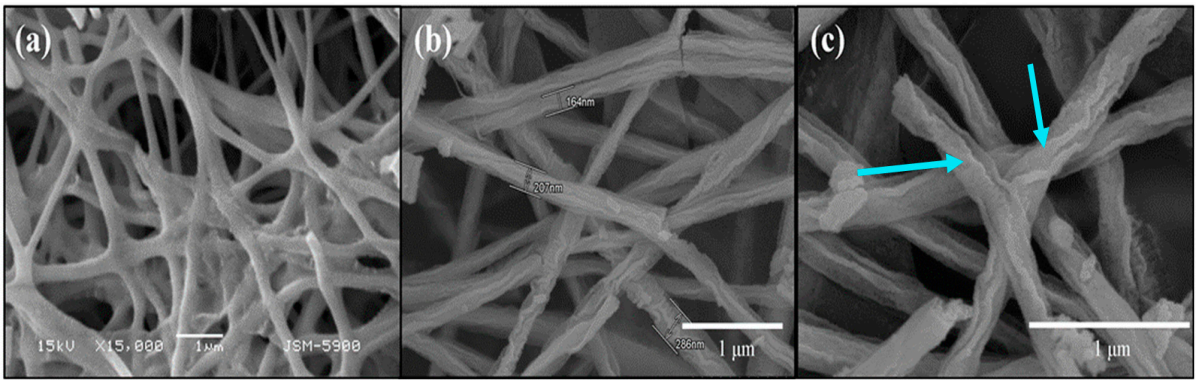

Figure 2. SEM profiles of (**a**) CeO_2 and (**b**,**c**) CeO_2-SnO_2 nanofibers at low and high magnifications after calcination at 500 °C. The arrows clearly show the characteristic sheath on composite NFs, which was absent for the bare CeO_2 NFs.

The arrows clearly show the characteristic sheath on the composite NFs, which was due to the presence of SnO_2 (Figure 2c). The different salt content significantly increased the solution conductivity, resulting in thinner electrospun fibers. Due to increased spinnability in the presence of Ce and Sn precursors, uniform nanofibers were generated. Consequently, it was observed that a different salt addition had a considerable impact on the spinnability of the polymer solution. Additionally, because of the increased conductivity, the electric field accelerated the ions and the interactions between the polymer and the salt resulted in a less compact polymer structure. Our findings show that when salt (Ce and S) ions were propelled by an electric field, the polymer chain followed the ions' motion, thereby decreasing the fiber diameter size. Analogous studies were reported for polymeric fibers by electrospinning in the presence of salts [59,60].

Figure 3a demonstrates the EDS results, which confirmed the presence of Ce, Sn, and O in the CeO_2-SnO_2 composite NFs. EDS analysis for the composite yielded an average atomic ratio of 1:0.15 for Ce/Sn. The detailed microstructure and morphology of composite NFs were further scanned using HR-TEM, the results of which are presented in Figure 3b. The surface consisted of two sets of lattices with spacings of 0.312 nm and 0.17 nm, corresponding to the interspace area between (111) and (211) of CeO_2 and SnO_2, respectively. It further verified the formation of a heterojunction between CeO_2 and SnO_2. The inset in Figure 3 demonstrates the low-resolution image of NFs. The TEM morphology of the CeO_2-SnO_2 NFs again showed that the average diameter of the composite NFs was 170 nm (*inset* of Figure 3). The corresponding selected area electron diffractions (SAED) arrangement of these NFs displayed a good ring pattern with no dislocations or imperfections, which can be attributed to the high crystalline phase of the composite sample, indicating the polycrystalline nature of the composite NFs (*inset* of Figure 3).

Figure 4 displays the FT-IR bands of the virgin CeO_2 and composite CeO_2-SnO_2 NFs. The existence of a strong band prior to 600 cm^{-1} could be assigned to the Ce-O-Ce stretching vibration [61] (Figure 4a). Both spectra revealed bands around 3450 cm^{-1} and 1637 cm^{-1} conforming to O–H widening vibration of the remaining water molecules and hydroxyl clusters. In the nanocomposite NFs spectra (Figure 4b), the occurrence of a band at 610 cm^{-1} corresponded to the stretching mode of SnO_2 [62]. The presence of both CeO_2 and SnO_2 peaks suggested the integration of these materials in the final composite NFs.

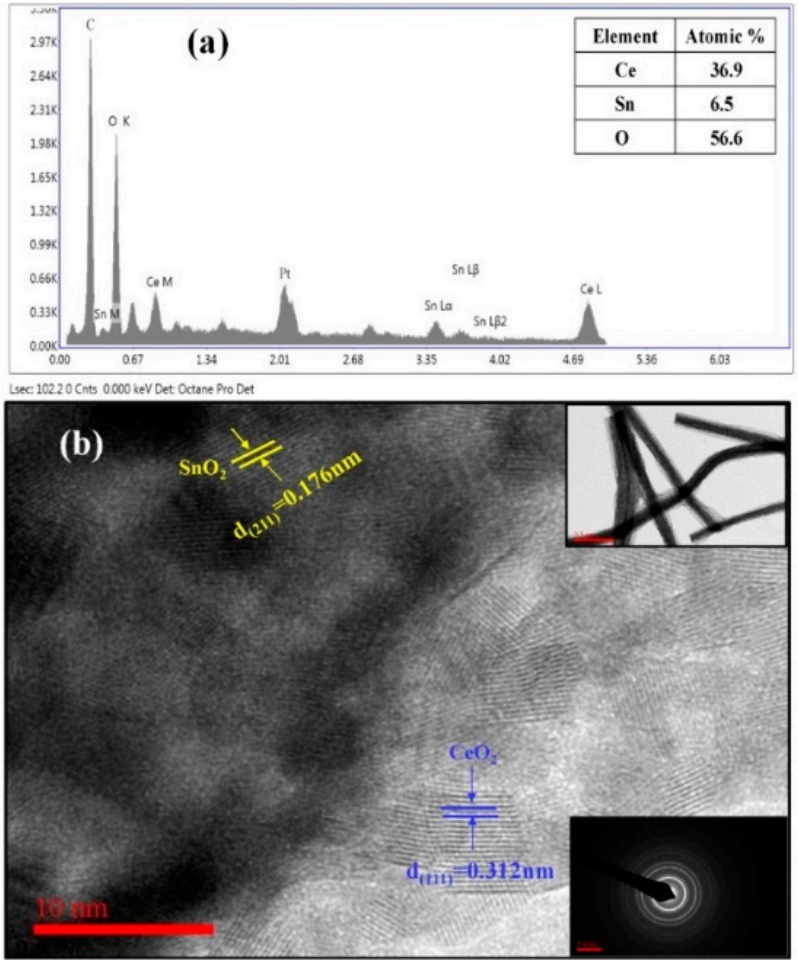

Figure 3. (**a**) EDX spectra and (**b**) HR-TEM image of the prepared CeO_2-SnO_2 composite NFs (the *inset* shows a low-resolution image and SAED pattern).

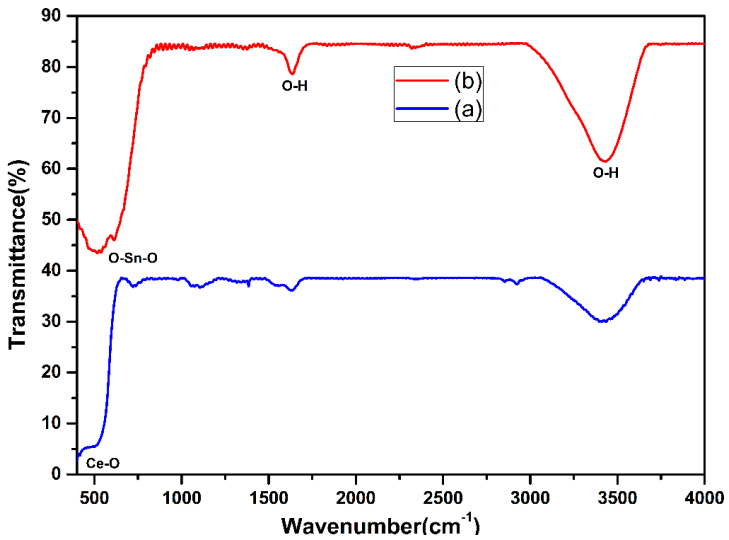

Figure 4. FT-IR configurations of the (**a**) CeO_2 and (**b**) CeO_2-SnO_2 NFs.

The optical characteristics of bare and composite NFs were assessed using UV-DRS (Figure 5). Figure 5A demonstrates the UV-DRS results of the CeO_2 and CeO_2-SnO_2 NFs, which show the absorption edge within the visible region. The spectrum of the CeO_2-SnO_2 composite presented a slight red shift, which coordinated well with pure CeO_2 and could

be ascribed to exciton partial leakage into the CeO_2 matrix. To estimate the band gaps of the prepared samples, the modified Kubelka–Munk function was plotted for $(Ah\nu)^2$ versus the energy of the exciting light ($h\nu$) using the following formula:

$$\alpha = \frac{\text{Constant}\left(h\nu - E_g\right)^n}{h\nu} \quad (2)$$

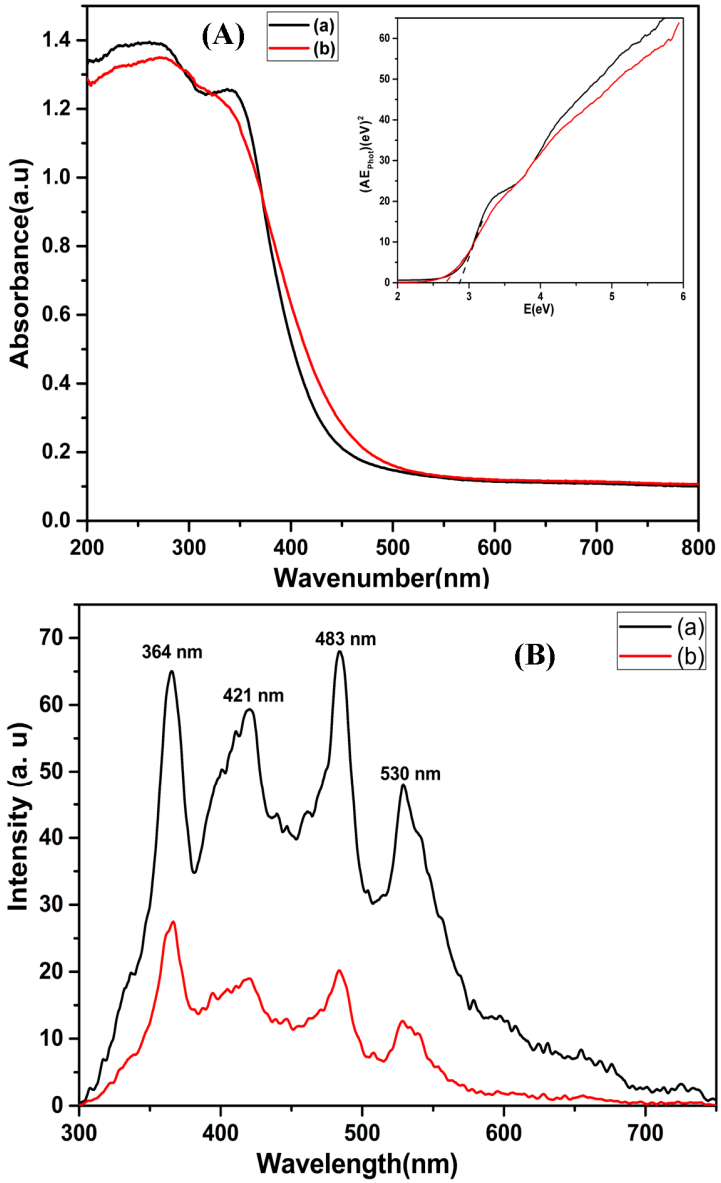

Figure 5. (**A**) UV-DRS pattern (*inset*: plot of the transformed Kubelka–Munk function versus the energy band gap) and (**B**) PL spectra of (**a**) CeO_2 and (**b**) CeO_2-SnO_2 composite NFs.

From the inset in Figure 5A, the calculated band gaps of the CeO_2 NFs and CeO_2-SnO_2 composite were found to be 2.87 eV and 2.67 eV, respectively. This means that the smaller band gap of CeO_2-SnO_2 composite NFs will harness more visible light than CeO_2 NFs. These results are consistent with an earlier report [63]. The PL emission spectra of the CeO_2 and CeO_2-SnO_2 composite samples were documented using an excitation wavelength (Figure 5B). The PL spectrum of CeO_2 had prominent peaks at 364, 421, 483, and 530 nm [64–66]. Moreover, the CeO_2-SnO_2 composite showed weaker emission peaks than CeO_2, indicating a lower recombination frequency of the photogenerated electron–hole pair.

The photoactivity of pure and composite nanofibers was assessed for the breakdown of MB dye under visible light (Figure 6). Figure 6A shows the MB concentration change calculated from its main absorption peak at 664 nm. From a comparative experiment, it can clearly be seen that CeO_2-SnO_2 composite photocatalyst displayed better photoactivity than the pure CeO_2 NFs (Figure 6B). After 125 min of visible light irradiation, the photodegradation effectivenesses of the CeO_2 and the CeO_2-SnO_2 composite photocatalysts for MB were 42% and 85%, respectively. The better photodegradation efficiency of the CeO_2-SnO_2 composite can be ascribed to the development of heterojunction between CeO_2 and SnO_2 and the parting of photogenerated electron–hole pairs.

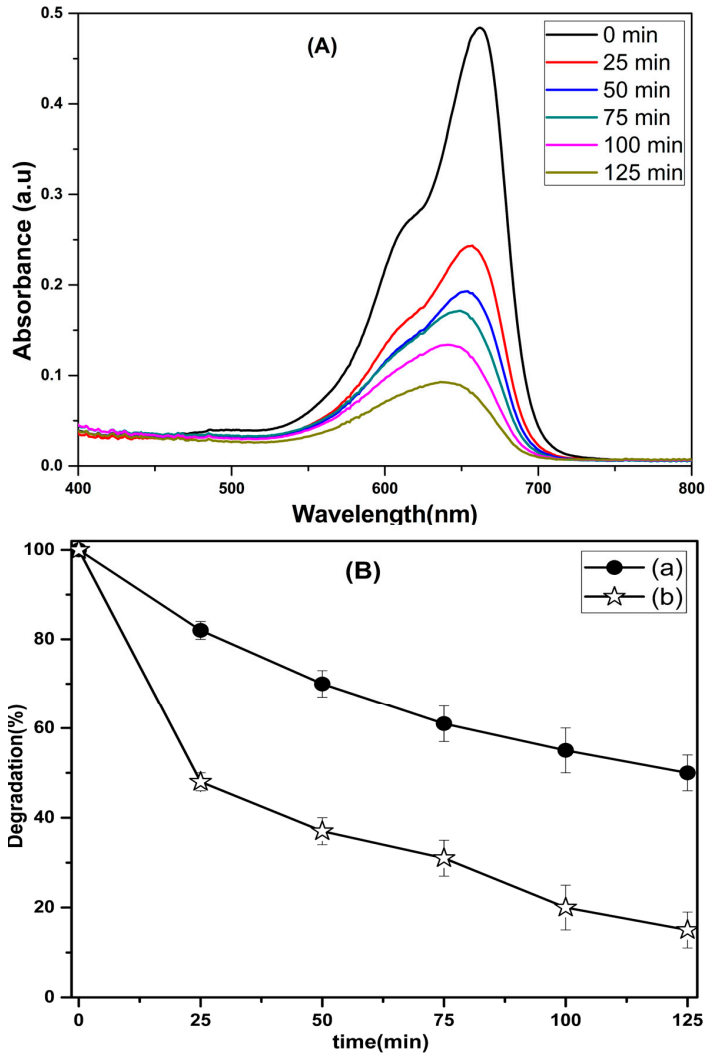

Figure 6. (**A**) Absorption spectra of MB dye using CeO_2-SnO_2 composite NFs for different periods and (**B**) relative photocatalytic action of (**a**) CeO_2 and (**b**) a CeO_2-SnO_2 nanocomposite for MB dye.

Figure 7 shows the reusability capacity of CeO_2-SnO_2 composite NFs for the degradation of MB dye. It was demonstrated that even after five cycles, the CeO_2-SnO_2 composite still exhibited good photocatalytic efficiency. It can be perceived that as the number of cycles increased, the composite photocatalytic activity marginally declined. The CeO_2-SnO_2 catalyst degraded 85% of the MB dye solution on its initial application, but after repeated applications (5th cycle), it had achieved a decolorization efficiency of 81%.

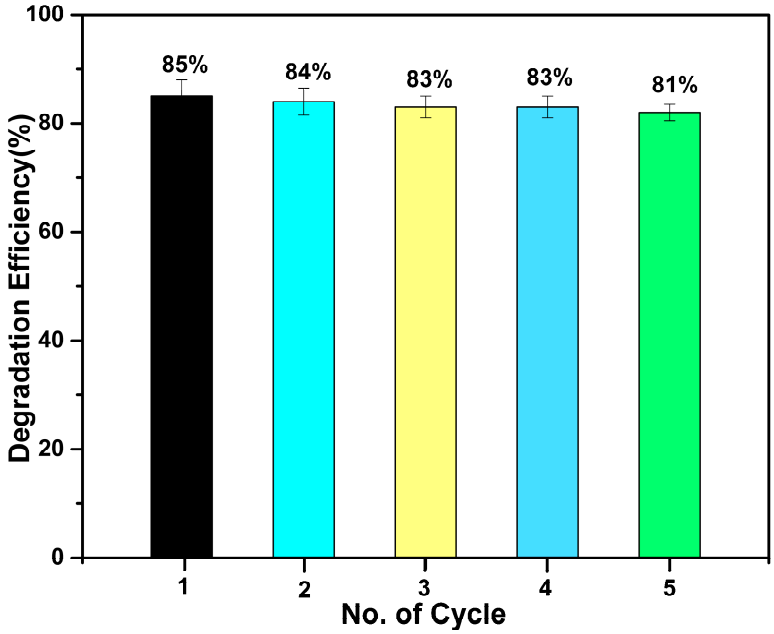

Figure 7. Recyclability studies of CeO_2-SnO_2 composite NFs for five consecutive cycles. Different color indicates different cycles

This shows that the CeO_2-SnO_2 catalyst was a reliable and efficient composite for dye degradation. Erstwhile, many similar studies also reported on composite nanomaterials for MB dye degradation (Table 1).

Table 1. Comparison of photocatalytic work results of different composite nanomaterials for MB dye degradation.

No.	Photocatalyst	Dye	Light Source	Time (min)	Degradation Efficiency (%)	Reference
1.	V_2O_5/RGO composite	MB	UV/visible	100	98.85	[4]
2.	HAP−$MnFe_2O_4$ nanocomposites	MB	Visible	150	88	[43]
3.	CeO_2-Cu_2O composite nanofibers	MB	UV/visible	180	92	[67]
4.	Mo/N−doped TiO_2 nanorods@CNFs	MB	Visible	180	79.8	[68]
5.	PANI nanotube@TiO_2 composite	MB	Visible	300	85	[69]
6.	C−doped ZnO nanofiber	MB	Solar	30	>95	[70]
7.	TiO_2/ZrO_2 composite nanofibers	MB	Visible	180	82.7	[71]
8.	TiO_2−decorated carbon nanofibers	MB	UV	180	97.4	[72]
9.	$\alpha-Fe_2O_3/Bi_2MoO_6$ composite nanofibers	MB	Sunlight	240	94.8	[73]
10.	ZnO/CdO alloy nanofibers	MB	Visible	270	>90	[74]
11.	Nanotextured CeO_2-SnO_2 composite fibers	MB	Visible	125	85	This study

A potential mechanism for photocatalytic MB degradation using a CeO_2-SnO_2 composite is hypothesized and illustrated in Figure 8. Under visible light irradiation, photons

are absorbed by the CeO_2 catalyst when energy is equivalent to or greater than the band gap. CeO_2 gets excited and generates electrons (e^-) and holes (h^+).

$$CeO_2 + h\nu \rightarrow (e_{CB}{}^-)_{CeO2} + (e_{VB}{}^+)_{CeO2} \quad (3)$$

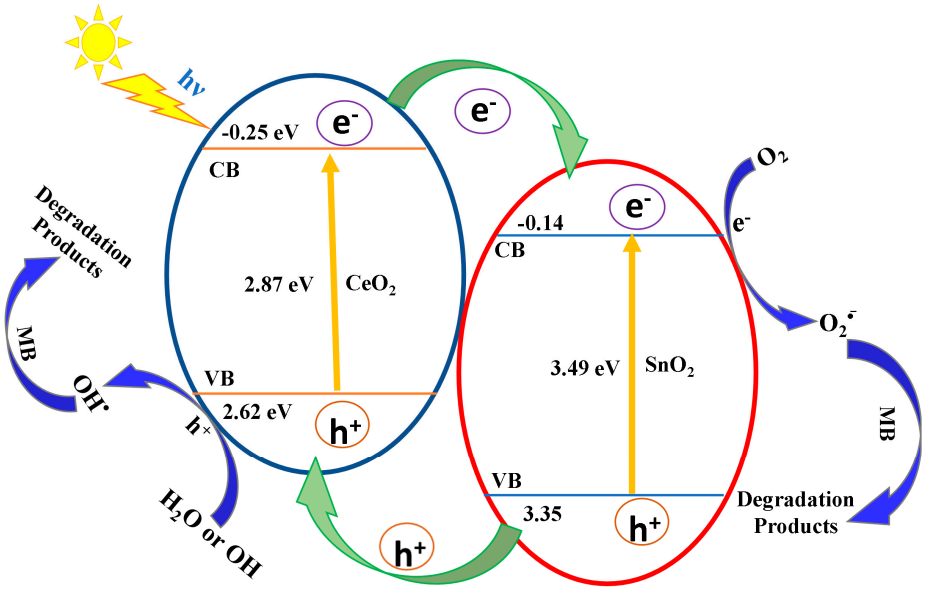

Figure 8. Schematic representation of the energy band configuration and electron−hole pair separation in CeO_2−SnO_2 NFs.

The photoexcited electrons are transported to the SnO_2, as the conduction band (CB) position of CeO_2 is more negative than SnO_2. Meanwhile, the transported electrons in the CB of SnO_2 will interact with dissolved oxygen molecules to generate superoxide radical anions ($O_2{}^-$). The superoxide radicals react with water and produce hydroperoxide radicals (HO_2) and hydroxyl radicals (OH). Subsequently, the holes on the valence band (VB) of SnO_2 migrate to the VB of the CeO_2 since the valence band potential of CeO_2 is more negative than that of SnO_2. Simultaneously, the generated h^+ can oxidize water molecules to produce OH. These radicals have a strong ability to degrade dye molecules (Figure 8). The MB dye is photo-oxidized into carbon dioxide and water molecules or inorganic ions as degradation products [63].

$$O_2 + (e_{CB}{}^-)_{SnO2} \rightarrow O_2{}^- \quad (4)$$

$$O_2{}^- + H_2O \rightarrow HO_2 + OH^- \quad (5)$$

$$h^+ + H_2O \rightarrow OH^- + H^+ \quad (6)$$

$$\text{MB dye + Radical species } (O_2{}^-, OH^-) \rightarrow \text{Degradation products } (CO_2 + H_2O) \quad (7)$$

Figure 9A demonstrates the cyclic voltammograms (CVs) of the pure CeO_2 NFs and CeO_2−SnO_2 NFs. The CeO_2−SnO_2 composite NFs indicated higher current values and better voltammetric shapes compared with pure CeO_2. The CeO_2−SnO_2 composite exhibited improved specific capacitance (413.9 Fg^{-1}) compared with the CeO_2 NFs (263.9 Fg^{-1}) at a scan rate of 10 mV/s. No redox peaks were observed in the CV of the bare CeO_2 NFs, which might have been due to the reason that there was little or no oxidation–reduction (corrosion or degradation) process going parallel to the double-layer charging. The presence of redox peaks in the CeO_2−SnO_2 composite NFs indicates that reversible and incessant faradaic oxidation–reduction responses were involved during the charging and discharging procedure [75,76]. It can be assumed that the electrochemical performances of composites were enhanced due to the synergistic effect between CeO_2 and SnO_2. Figure 9B shows the CV curves for different scan rates for the CeO_2−SnO_2 composite. The CeO_2−SnO_2 composite

NFs confirmed elevated specific capacitance values of 413.9, 294.94, 147.6, and 16.1 F/g at scan rates of 5, 10, 50, and 100 mVs^{-1}, correspondingly.

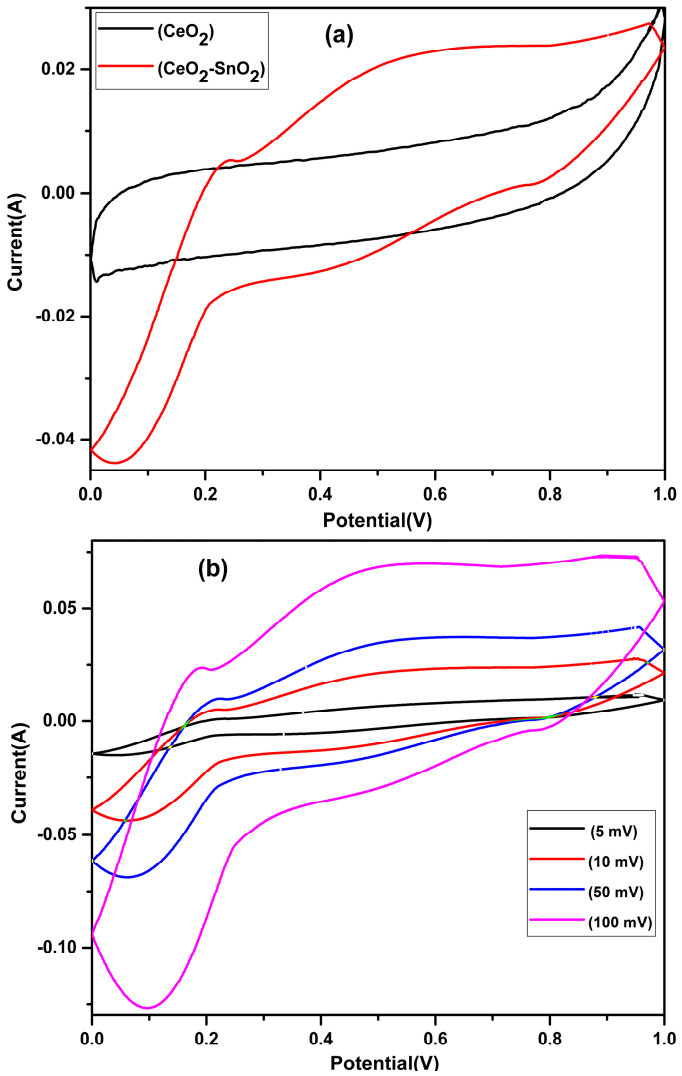

Figure 9. (**a**) Cyclic voltammograms of the CeO_2 and CeO_2-SnO_2 NFs electrodes at a scanning rate of 5 mV/s and (**b**) CVs of CeO_2-SnO_2 NFs at different scanning rates.

In the antibacterial bioassay, CeO_2 NFs and CeO_2-SnO_2 composite NFs were tested against specified bacteria using an agar diffusion experiment at various doses. The CeO_2 and CeO_2-SnO_2 composite NFs were found to be the most promising, with MICs of 50 µg/mL for *E. coli* (Figure 10). The augmented activity of the CeO_2-SnO_2 composite NFs might be attributed to their form and wide surface area [77], as well as the synergistic influence of CeO_2 and SnO_2 in the composite NFs. However, the antibacterial activities of the virgin CeO_2 NFs and CeO_2-SnO_2 composite NFs were identical at a low concentration, the antibacterial impact varied with the increase in concentration and incubation time. The chemical components of the CeO_2-SnO_2 composite NFs primarily reacted with the bacterial outer cell wall before diffusing inside the inner wall, producing disarray and leaking through the disturbance in the inner cell content and distortion. A few previous investigations also showed that CeO_2 nanoparticles have exceptional antibacterial activity [44,45]. In particular, some studies found that CeO_2 has an antibacterial effect on *S. aureus* [46,47]. Furthermore, agar diffusion and microdilution experiments were utilized in certain studies to examine and validate *P. aeruginosa*'s sensitivity to CeO_2 [48]. Similarly, SnO_2 also attracted interest as an effective antibacterial, where it was shown to inhibit the

development of several bacterial strains, such as *S. aureus* and *E. coli* [49,50]. Furthermore, it was observed that SnO_2 supplemented with transition metal ions effectively disinfects microorganisms and possesses potent antibacterial activities [51–53].

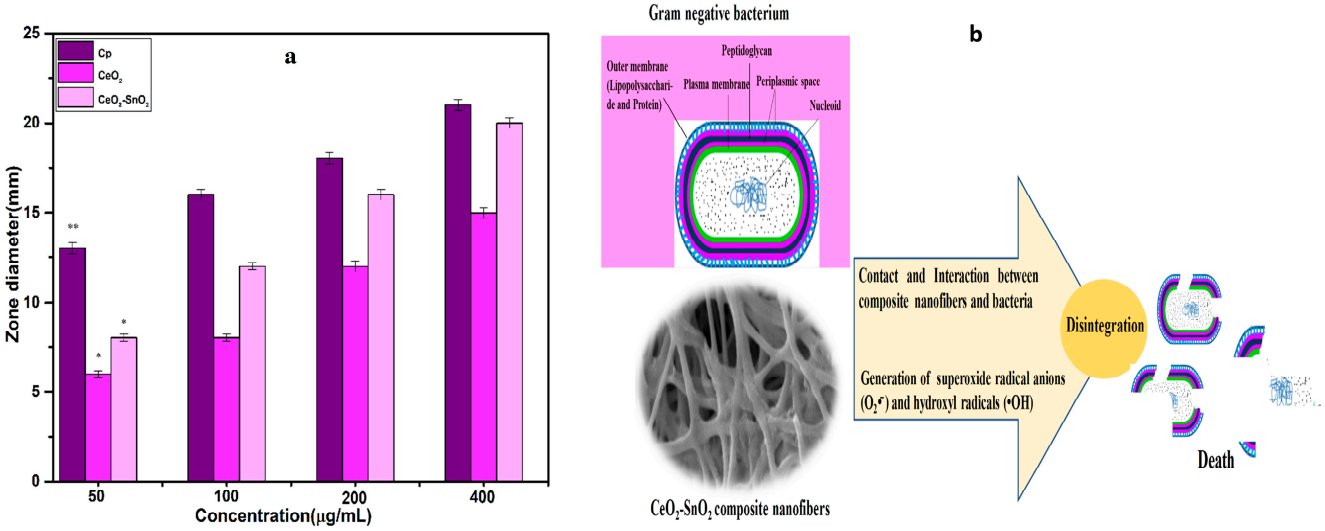

Figure 10. (**a**) *E. coli* susceptibility to CeO_2 NFs and CeO_2-SnO_2 composite NFs (50–400 μg/mL). Ciprofloxacin was used as the standard antibiotic. The data are given as mean values and standard deviations of three replicates. * $p < 0.005$ and ** $p < 0.01$ vs. control. (**b**) Pictorial illustration of bacterial death and disintegration.

4. Conclusions

In summary, CeO_2-SnO_2 composite NFs were prepared via electrospinning. As aforementioned, many strategies for removing MB and other textile dyes from industrial effluent were reported in the literature. However, in the present study, the photocatalysis approach was used. The addition of SnO_2 to CeO_2 significantly improved the photocatalytic MB degradation property and photoelectrochemical performance. After 125 min of irradiation, a photodegradation efficiency of 85% was achieved using the CeO_2-SnO_2 composite photocatalyst. Moreover, the CeO_2-SnO_2 composite NFs also showed higher specific capacitance. It is believed that these CeO_2-SnO_2 composite NFs with excellent photoactivity and electrochemical performance can be very promising for high-performance electrode materials in supercapacitors and as an efficient alternative photocatalyst. Rationally, due to their distinctive functional mechanism towards pathogens via reversible oxidation state transition between Ce(III) and Ce(IV), (IV) CeO_2 nanoparticles with lower toxicity work as powerful antibacterial agents as well. The outcome of this study indicates the prospects of CeO_2-SnO_2 composite NFs to be exploited as an antimicrobial material, an electrode, and as a visible light active photocatalyst, which would greatly aid in the environmental cleanup process.

Author Contributions: Conceptualization, J.S.A., M.S.H. and T.A.; methodology, J.S.A. and M.S.H.; software, M.A.M.A.; validation, A.F.S. and M.F.; formal analysis, H.Y.K.; investigation, T.A.; resources, F.A.S.; data curation, A.F.S. and M.F.; writing—original draft preparation, M.S.H., T.A. and J.S.A.; writing—review and editing, T.A. and F.A.S. All authors have read and agreed to the published version of the manuscript.

Funding: The authors are thankful to the Deanship of Scientific Research at Najran University for funding this work under the General Research Funding program "Functional Composite Materials for Water Remediation", grant code (NU/DRP/SERC/12/45).

Data Availability Statement: Data is included in the main text.

Acknowledgments: The authors are thankful to the Deanship of Scientific Research at Najran University for funding this work under the General Research Funding program, grant code (NU/DRP/SERC/12/45).

Conflicts of Interest: The authors declare no conflict of interest.

References

1. Guo, W.; Luo, H.; Jiang, Z.; Fang, D.; Chi, J.; Shangguan, W.; Wang, Z.; Wang, L.; Lee, A.F. Ge-doped cobalt oxide for electrocatalytic and photocatalytic water splitting. *ACS Catal.* **2022**, *12*, 12000–12013. [CrossRef]
2. Hunge, Y.M.; Yadav, A.A.; Kang, S.-W.; Lim, S.J.; Kim, H. Visible light activated MoS_2/ZnO composites for photocatalytic degradation of ciprofloxacin antibiotic and hydrogen production. *J. Photochem. Photobiol. A Chem.* **2023**, *434*, 114250. [CrossRef]
3. Das, T.K.; Das, N.C. Advances on catalytic reduction of 4-nitrophenol by nanostructured materials as benchmark reaction. *Int. Nano Lett.* **2022**, *12*, 223–242. [CrossRef]
4. Yadav, A.A.; Hunge, Y.M.; Kang, S.-W.; Fujishima, A.; Terashima, C. Enhanced Photocatalytic Degradation Activity Using the V_2O_5/RGO Composite. *Nanomaterials* **2023**, *13*, 338. [CrossRef]
5. Fong, W.M.; Affam, A.C.; Chung, W.C. Synthesis of Ag/Fe/CAC for colour and COD removal from methylene blue dye wastewater. *Int. J. Environ. Sci. Technol.* **2020**, *17*, 3485–3494. [CrossRef]
6. Han, T.H.; Khan, M.M.; Kalathil, S.; Lee, J.; Cho, M.H. Simultaneous enhancement of methylene blue degradation and power generation in a microbial fuel cell by gold nanoparticles. *Ind. Eng. Chem. Res.* **2013**, *52*, 8174–8181. [CrossRef]
7. Khan, I.; Saeed, K.; Zekker, I.; Zhang, B.; Hendi, A.H.; Ahmad, A.; Ahmad, S.; Zada, N.; Ahmad, H.; Shah, L.A. Review on methylene blue: Its properties, uses, toxicity and photodegradation. *Water* **2022**, *14*, 242. [CrossRef]
8. Abdelrahman, E.A.; Hegazey, R.; El-Azabawy, R.E. Efficient removal of methylene blue dye from aqueous media using Fe/Si, Cr/Si, Ni/Si, and Zn/Si amorphous novel adsorbents. *J. Mater. Res. Technol.* **2019**, *8*, 5301–5313. [CrossRef]
9. Jawad, A.H.; Abdulhameed, A.S.; Mastuli, M.S. Acid-factionalized biomass material for methylene blue dye removal: A comprehensive adsorption and mechanism study. *J. Taibah Univ. Sci.* **2020**, *14*, 305–313. [CrossRef]
10. Wang, Y.; Peng, Q.; Akhtar, N.; Chen, X.; Huang, Y. Microporous carbon material from fish waste for removal of methylene blue from wastewater. *Water Sci. Technol.* **2020**, *81*, 1180–1190. [CrossRef]
11. Zamel, D.; Hassanin, A.H.; Ellethy, R.; Singer, G.; Abdelmoneim, A. Novel bacteria-immobilized cellulose acetate/poly (ethylene oxide) nanofibrous membrane for wastewater treatment. *Sci. Rep.* **2019**, *9*, 18994. [CrossRef] [PubMed]
12. Cabral, J.P. Water microbiology. Bacterial pathogens and water. *Int. J. Environ. Res. Public Health* **2010**, *7*, 3657–3703. [CrossRef] [PubMed]
13. Hunge, Y.; Yadav, A.; Kang, S.-W.; Kim, H. Facile synthesis of multitasking composite of Silver nanoparticle with Zinc oxide for 4-nitrophenol reduction, photocatalytic hydrogen production, and 4-chlorophenol degradation. *J. Alloys Compd.* **2022**, *928*, 167133. [CrossRef]
14. Chandra, R.; Nath, M. Controlled synthesis of AgNPs@ ZIF-8 composite: Efficient heterogeneous photocatalyst for degradation of methylene blue and congo red. *J. Water Process Eng.* **2020**, *36*, 101266. [CrossRef]
15. Hunge, Y.M.; Yadav, A.A.; Kang, S.-W.; Mohite, B.M. Role of Nanotechnology in Photocatalysis Application. *Recent Pat. Nanotechnol.* **2023**, *17*, 5–7. [CrossRef] [PubMed]
16. Muhd Julkapli, N.; Bagheri, S.; Bee Abd Hamid, S. Recent advances in heterogeneous photocatalytic decolorization of synthetic dyes. *Sci. World J.* **2014**, *2014*, 692307. [CrossRef] [PubMed]
17. Alorabi, A.Q.; Hassan, M.S.; Algethami, J.S.; Baghdadi, N.E. Synthesis and characterization of Ag-$AgVO_3$/Cu_2O heterostructure with improved visible-light photocatalytic performance. *Sci. Prog.* **2021**, *104*, 00368504211050300. [CrossRef]
18. Zhang, H.; Zhang, F.; Wei, Y.; Miao, Q.; Li, A.; Zhao, Y.; Yuan, Y.; Jin, N.; Li, G. Controllable Design and Preparation of Hollow Carbon-Based Nanotubes for Asymmetric Supercapacitors and Capacitive Deionization. *ACS Appl. Mater. Interfaces* **2021**, *13*, 21217–21230. [CrossRef]
19. Han, Y.; Sun, C.; Gao, K.; Ding, S.; Miao, Z.; Zhao, J.; Yang, Z.; Wu, P.; Huang, J.; Li, Z. Heterovalent oxynitride GaZnON nanowire as novel flexible anode for lithium-ion storage. *Electrochim. Acta* **2022**, *408*, 139931. [CrossRef]
20. Hassan, M.S.; Amna, T.; Alqarni, L.S.; Alqahtani, H.S.; Alnaam, Y.A.; Almusabi, S.; Alzharani, A.A. High aspect ratio TiO_2–Mn_3O_4 heterostructure: Proficient nanorods for pathogen inhibition and supercapacitor application. *Mater. Sci. Technol.* **2023**, 1–10. [CrossRef]
21. Gao, S.; Jiang, J.; Li, X.; Ye, F.; Fu, Y.; Zhao, L. Electrospun polymer-free nanofibers incorporating hydroxypropyl-β-cyclodextrin/Difenoconazole via supramolecular assembly for antifungal activity. *J. Agric. Food Chem.* **2021**, *69*, 5871–5881. [CrossRef] [PubMed]
22. Ding, D.; Li, Z.; Yu, S.; Yang, B.; Yin, Y.; Zan, L.; Myung, N.V. Piezo-photocatalytic flexible PAN/TiO_2 composite nanofibers for environmental remediation. *Sci. Total Environ.* **2022**, *824*, 153790. [CrossRef]
23. Han, W.-H.; Li, X.; Yu, G.-F.; Wang, B.-C.; Huang, L.-P.; Wang, J.; Long, Y.-Z. Recent Advances in the Food Application of Electrospun Nanofibers. *J. Ind. Eng. Chem.* **2022**, *110*, 15–26. [CrossRef]
24. Xue, C.; Liu, Y.; Zhao, J.; Li, X.; Zhang, J.; Zhang, J. Nitrogen-doped carbon nanofibers derived from phenolic-resin-based analogues for high-performance lithium-ion batteries. *Solid State Ion.* **2022**, *376*, 115854. [CrossRef]

25. Payan, A.; Aghdam, N.C.; Soltan, J. Catalytic oxidation of acetone in air over Ag modified CeO_2 catalysts under VUV irradiation: Comparison of different treatment process, performance, and mechanism studies. *J. Environ. Chem. Eng.* **2022**, *10*, 107253. [CrossRef]
26. Hassan, M.S.; Khan, R.; Amna, T.; Yang, J.; Lee, I.-H.; Sun, M.-Y.; EL-Newehy, M.H.; Al-Deyab, S.S.; Khil, M.-S. The influence of synthesis method on size and toxicity of CeO2 quantum dots: Potential in the environmental remediation. *Ceram. Int.* **2016**, *42*, 576–582. [CrossRef]
27. Das, T.K.; Remanan, S.; Ghosh, S.; Ghosh, S.K.; Das, N.C. Efficient synthesis of catalytic active silver nanoparticles illuminated cerium oxide nanotube: A mussel inspired approach. *Environ. Nanotechnol. Monit. Manag.* **2021**, *15*, 100411. [CrossRef]
28. Dong, F.; Tanabe, T.; Takahashi, N.; Shinjoh, H. Investigation of the effective oxygen storage and release performances on the Pt/CeO_2-ZrO_2 catalysts by breakthrough method. *Catal. Today* **2019**, *332*, 259–266. [CrossRef]
29. Chu, Z.; Li, J.; Lan, Y.-P.; Chen, C.; Yang, J.; Ning, D.; Xia, X.; Mao, X. KCl–LiCl molten salt synthesis of $LaOCl/CeO_2$-g-C_3N_4 with excellent photocatalytic-adsorbed removal performance for organic dye pollutant. *Ceram. Int.* **2022**, *48*, 15439–15450. [CrossRef]
30. Zhang, Y.; Wu, M.; Wang, Y.; Zhao, X.; Leung, D.Y. Low-cost and efficient Mn/CeO_2 catalyst for photocatalytic VOCs degradation via scalable colloidal solution combustion synthesis method. *J. Mater. Sci. Technol.* **2022**, *116*, 169–179. [CrossRef]
31. Liu, Z.; Zheng, J.; Duan, L.; Zhu, Z. Biomass-assisted synthesis of CeO_2 nanorods for CO_2 photoreduction under visible light. *ACS Appl. Nano Mater.* **2021**, *4*, 4226–4237. [CrossRef]
32. Xue, Z.; Lv, L.; Tian, Y.; Tan, S.; Ma, Q.; Tao, K.; Han, L. Co_3S_4 nanoplate arrays decorated with oxygen-deficient CeO_2 nanoparticles for supercapacitor applications. *ACS Appl. Nano Mater.* **2021**, *4*, 3033–3043. [CrossRef]
33. AL-Shwaiman, H.A.; Akshhayya, C.; Syed, A.; Bahkali, A.H.; Elgorban, A.M.; Das, A.; Varma, R.S.; Khan, S.S. Fabrication of intimately coupled $CeO_2/ZnFe_2O_4$ nano-heterojunction for visible-light photocatalysis and bactericidal application. *Mater. Chem. Phys.* **2022**, *279*, 125759. [CrossRef]
34. Munawar, T.; Mukhtar, F.; Nadeem, M.S.; Manzoor, S.; Ashiq, M.N.; Mahmood, K.; Batool, S.; Hasan, M.; Iqbal, F. Fabrication of dual Z-scheme TiO_2-WO_3-CeO_2 heterostructured nanocomposite with enhanced photocatalysis, antibacterial, and electrochemical performance. *J. Alloys Compd.* **2021**, *898*, 162779. [CrossRef]
35. Zheng, J.; Wang, J.; Qu, J.; Wu, M.; Xu, Z. CeO_2/Ni-Al layered double hydroxide composite electrode for the enhancement of specific capacitance and capacitance retention performance. *Appl. Clay Sci.* **2022**, *216*, 106370. [CrossRef]
36. Xie, A.; Wang, H.; Zhu, Z.; Zhang, W.; Li, X.; Wang, Q.; Luo, S. Mesoporous CeO_2-α-MnO_2-reduced graphene oxide composite with ultra-high stability as a novel electrode material for supercapacitor. *Surf. Interfaces* **2021**, *25*, 101177. [CrossRef]
37. Yin, L.; Xu, J.; Zhang, B.; Wang, L.; Tao, W.; Teng, X.; Ning, W.; Zhang, Z. A facile fabrication of highly dispersed CeO_2/SiO_2 aerogel composites with high adsorption desulfurization performance. *Chem. Eng. J.* **2022**, *428*, 132581. [CrossRef]
38. Lu, Y.; Duan, L.; Sun, Z.; Chen, J. Flame spray pyrolysis synthesized CuO–CeO_2 composite for catalytic combustion of C_3H_6. *Proc. Combust. Inst.* **2021**, *38*, 6513–6520. [CrossRef]
39. Thirunavukkarasu, A.; Nithya, R. Adsorption of acid orange 7 using green synthesized CaO/CeO_2 composite: An insight into kinetics, equilibrium, thermodynamics, mass transfer and statistical models. *J. Taiwan Inst. Chem. Eng.* **2020**, *111*, 44–62. [CrossRef]
40. Van, K.N.; Huu, H.T.; Thi, V.N.N.; Le Thi, T.L.; Truong, D.H.; Truong, T.T.; Dao, N.N.; Vo, V.; Vasseghian, Y. Facile construction of S-scheme SnO_2/g-C_3N_4 photocatalyst for improved photoactivity. *Chemosphere* **2022**, *289*, 133120. [CrossRef]
41. Panday, M.; Upadhyay, G.K.; Purohit, L. Sb incorporated SnO_2 nanostructured thin films for CO_2 gas sensing and humidity sensing applications. *J. Alloys Compd.* **2022**, *904*, 164053. [CrossRef]
42. Qureshi, A.A.; Javed, S.; Javed, H.M.A.; Akram, A.; Mustafa, M.S.; Ali, U.; Nisar, M.Z. Facile formation of SnO_2–TiO_2 based photoanode and Fe_3O_4@ rGO based counter electrode for efficient dye-sensitized solar cells. *Mater. Sci. Semicond. Process.* **2021**, *123*, 105545. [CrossRef]
43. Algethami, J.S.; Hassan, M.S.; Alorabi, A.Q.; Alhemiary, N.A.; Fallatah, A.M.; Alnaam, Y.; Almusabi, S.; Amna, T. Manganese Ferrite–Hydroxyapatite Nanocomposite Synthesis: Biogenic Waste Remodeling for Water Decontamination. *Nanomaterials* **2022**, *12*, 1631. [CrossRef] [PubMed]
44. Farias, I.A.P.; Santos, C.C.L.d.; Sampaio, F.C. Antimicrobial activity of cerium oxide nanoparticles on opportunistic microorganisms: A systematic review. *BioMed. Res. Int.* **2018**, *2018*, 1923606. [CrossRef]
45. Pop, O.L.; Mesaros, A.; Vodnar, D.C.; Suharoschi, R.; Tăbăran, F.; Mageruşan, L.; Tódor, I.S.; Diaconeasa, Z.; Balint, A.; Ciontea, L. Cerium oxide nanoparticles and their efficient antibacterial application in vitro against gram-positive and gram-negative pathogens. *Nanomaterials* **2020**, *10*, 1614. [CrossRef] [PubMed]
46. Reddy Yadav, L.; Manjunath, K.; Archana, B.; Madhu, C.; Raja Naika, H.; Nagabhushana, H.; Kavitha, C.; Nagaraju, G. Fruit juice extract mediated synthesis of CeO_2 nanoparticles for antibacterial and photocatalytic activities. *Eur. Phys. J. Plus* **2016**, *131*, 1–10. [CrossRef]
47. Gopinath, K.; Karthika, V.; Sundaravadivelan, C.; Gowri, S.; Arumugam, A. Mycogenesis of cerium oxide nanoparticles using Aspergillus niger culture filtrate and their applications for antibacterial and larvicidal activities. *J. Nanostructure Chem.* **2015**, *5*, 295–303. [CrossRef]
48. Ravishankar, T.N.; Ramakrishnappa, T.; Nagaraju, G.; Rajanaika, H. Synthesis and characterization of CeO_2 nanoparticles via solution combustion method for photocatalytic and antibacterial activity studies. *ChemistryOpen* **2015**, *4*, 146–154. [CrossRef]

49. Phukan, A.; Bhattacharjee, R.P.; Dutta, D.K. Stabilization of SnO_2 nanoparticles into the nanopores of modified Montmorillonite and their antibacterial activity. *Adv. Powder Technol.* **2017**, *28*, 139–145. [CrossRef]
50. Kumari, M.M.; Philip, D. Synthesis of biogenic SnO_2 nanoparticles and evaluation of thermal, rheological, antibacterial and antioxidant activities. *Powder Technol.* **2015**, *270*, 312–319. [CrossRef]
51. Chandran, D.; Nair, L.S.; Balachandran, S.; Rajendra Babu, K.; Deepa, M. Structural, optical, photocatalytic, and antimicrobial activities of cobalt-doped tin oxide nanoparticles. *J. Sol-Gel Sci. Technol.* **2015**, *76*, 582–591. [CrossRef]
52. Nasir, Z.; Shakir, M.; Wahab, R.; Shoeb, M.; Alam, P.; Khan, R.H.; Mobin, M. Co-precipitation synthesis and characterization of Co doped SnO_2 NPs, HSA interaction via various spectroscopic techniques and their antimicrobial and photocatalytic activities. *Int. J. Biol. Macromol.* **2017**, *94*, 554–565. [CrossRef] [PubMed]
53. Qamar, M.A.; Shahid, S.; Khan, S.A.; Zaman, S.; Sarwar, M.N. Synthesis characterization, optical and antibacterial studies of Co-doped SnO_2 nanoparticles. *Dig. J. Nanomater. Biostruct.* **2017**, *12*, 1127–1135.
54. Hassan, M.S.; Amna, T.; Yang, O.-B.; El-Newehy, M.H.; Al-Deyab, S.S.; Khil, M.-S. Smart copper oxide nanocrystals: Synthesis, characterization, electrochemical and potent antibacterial activity. *Colloids Surf. B Biointerfaces* **2012**, *97*, 201–206. [CrossRef] [PubMed]
55. Jorgensen, J.H.; Hindler, J.F.; Reller, L.B.; Weinstein, M.P. New consensus guidelines from the Clinical and Laboratory Standards Institute for antimicrobial susceptibility testing of infrequently isolated or fastidious bacteria. *Clin. Infect. Dis.* **2007**, *44*, 280–286. [CrossRef]
56. Xue, J.; Xie, J.; Liu, W.; Xia, Y. Electrospun nanofibers: New concepts, materials, and applications. *Acc. Chem. Res.* **2017**, *50*, 1976–1987. [CrossRef]
57. Nilchi, A.; Yaftian, M.; Aboulhasanlo, G.; Rasouli Garmarodi, S. Adsorption of selected ions on hydrous cerium oxide. *J. Radioanal. Nucl. Chem.* **2009**, *279*, 65–74. [CrossRef]
58. Bao, H.; Zhang, Z.; Hua, Q.; Huang, W. Compositions, structures, and catalytic activities of CeO_2@ Cu_2O nanocomposites prepared by the template-assisted method. *Langmuir* **2014**, *30*, 6427–6436. [CrossRef]
59. Wang, B.-B.; Wang, X.-D.; Wang, T.-H. Microscopic mechanism for the effect of adding salt on electrospinning by molecular dynamics simulations. *Appl. Phys. Lett.* **2014**, *105*, 121906. [CrossRef]
60. Topuz, F.; Abdulhamid, M.A.; Holtzl, T.; Szekely, G. Nanofiber engineering of microporous polyimides through electrospinning: Influence of electrospinning parameters and salt addition. *Mater. Des.* **2021**, *198*, 109280. [CrossRef]
61. Ho, C.; Yu, J.C.; Kwong, T.; Mak, A.C.; Lai, S. Morphology-controllable synthesis of mesoporous CeO_2 nano- and microstructures. *Chem. Mater.* **2005**, *17*, 4514–4522. [CrossRef]
62. Wan, W.; Li, Y.; Ren, X.; Zhao, Y.; Gao, F.; Zhao, H. 2D SnO_2 nanosheets: Synthesis, characterization, structures, and excellent sensing performance to ethylene glycol. *Nanomaterials* **2018**, *8*, 112. [CrossRef] [PubMed]
63. Manibalan, G.; Murugadoss, G.; Thangamuthu, R.; Kumar, R.M.; Jayavel, R.; Kumar, M.R. Enhanced photocatalytic performance of heterostructure CeO_2–SnO_2 nanocomposite via hydrothermal route. *Mater. Res. Express* **2019**, *6*, 075032. [CrossRef]
64. Subhan, A.; Ahmed, T.; Awal, M.R.; Kim, B.M. Structure and photoluminescence studies of CeO_2 $CuAlO_2$ mixed metal oxide fabricated by co-precipitation method. *Spectrochim. Acta Part A Mol. Biomol. Spectrosc.* **2015**, *135*, 466–471. [CrossRef] [PubMed]
65. Malleshappa, J.; Nagabhushana, H.; Prasad, B.D.; Sharma, S.; Vidya, Y.; Anantharaju, K. Structural, photoluminescence and thermoluminescence properties of CeO2 nanoparticles. *Optik* **2016**, *127*, 855–861. [CrossRef]
66. Kumar, S.; Ojha, A.K.; Patrice, D.; Yadav, B.S.; Materny, A. One-step in situ synthesis of CeO_2 nanoparticles grown on reduced graphene oxide as an excellent fluorescent and photocatalyst material under sunlight irradiation. *Phys. Chem. Chem. Phys.* **2016**, *18*, 11157–11167. [CrossRef]
67. Chae, B.W.; Amna, T.; Hassan, M.S.; Al-Deyab, S.S.; Khil, M.-S. CeO_2-Cu_2O composite nanofibers: Synthesis, characterization photocatalytic and electrochemical application. *Adv. Powder Technol.* **2017**, *28*, 230–235. [CrossRef]
68. Qiu, J.; Liu, F.; Yue, C.; Ling, C.; Li, A. A recyclable nanosheet of Mo/N-doped TiO_2 nanorods decorated on carbon nanofibers for organic pollutants degradation under simulated sunlight irradiation. *Chemosphere* **2019**, *215*, 280–293. [CrossRef]
69. Jeong, W.-H.; Amna, T.; Ha, Y.-M.; Hassan, M.S.; Kim, H.-C.; Khil, M.-S. Novel PANI nanotube@ TiO_2 composite as efficient chemical and biological disinfectant. *Chem. Eng. J.* **2014**, *246*, 204–210. [CrossRef]
70. Gadisa, B.T.; Appiah-Ntiamoah, R.; Kim, H. In-situ derived hierarchical ZnO/Zn-C nanofiber with high photocatalytic activity and recyclability under solar light. *Appl. Surf. Sci.* **2019**, *491*, 350–359. [CrossRef]
71. Yasin, A.S.; Obaid, M.; El-Newehy, M.H.; Al-Deyab, S.S.; Barakat, N.A. Influence of $TixZr_{(1-x)}O_2$ nanofibers composition on the photocatalytic activity toward organic pollutants degradation and water splitting. *Ceram. Int.* **2015**, *41*, 11876–11885. [CrossRef]
72. Wang, H.; Huang, X.; Li, W.; Gao, J.; Xue, H.; Li, R.K.; Mai, Y.-W. TiO_2 nanoparticle decorated carbon nanofibers for removal of organic dyes. *Colloids Surf. A Physicochem. Eng. Asp.* **2018**, *549*, 205–211. [CrossRef]
73. Zhao, J.; Lu, Q.; Wang, Q.; Ma, Q. α-Fe_2O_3 nanoparticles on Bi_2MoO_6 nanofibers: One-dimensional heterostructures synergistic system with enhanced photocatalytic activity. *Superlattices Microstruct.* **2016**, *91*, 148–157. [CrossRef]
74. Yousef, A.; Barakat, N.A.; Amna, T.; Unnithan, A.R.; Al-Deyab, S.S.; Kim, H.Y. Influence of CdO-doping on the photoluminescence properties of ZnO nanofibers: Effective visible light photocatalyst for waste water treatment. *J. Lumin.* **2012**, *132*, 1668–1677. [CrossRef]
75. Zhou, F.; Liu, Q.; Kang, D.; Gu, J.; Zhang, W.; Zhang, D. A 3D hierarchical hybrid nanostructure of carbon nanotubes and activated carbon for high-performance supercapacitors. *J. Mater. Chem. A* **2014**, *2*, 3505–3512. [CrossRef]

76. Priyadharsan, A.; Vasanthakumar, V.; Karthikeyan, S.; Raj, V.; Shanavas, S.; Anbarasan, P.M. Multi-functional properties of ternary CeO_2/SnO_2/rGO nanocomposites: Visible light driven photocatalyst and heavy metal removal. *J. Photochem. Photobiol. A Chem.* **2017**, *346*, 32–45. [CrossRef]
77. Ann, L.C.; Mahmud, S.; Bakhori, S.K.M.; Sirelkhatim, A.; Mohamad, D.; Hasan, H.; Seeni, A.; Rahman, R.A. Antibacterial responses of zinc oxide structures against Staphylococcus aureus, Pseudomonas aeruginosa and Streptococcus pyogenes. *Ceram. Int.* **2014**, *40*, 2993–3001. [CrossRef]